P341

On the Contribution of Head Waves to Full Waveform Inversion

V.V. Kazei* (St. Petersburg University), A.V. Ponomarenko (St. Petersburg University), V.N. Troyan (St. Petersburg University), B.M. Kashtan (St. Petersburg University) & W.A. Mulder (Shell Global Solutions International BV / Delft University of Technology)

SUMMARY

Full waveform inversion suffers from local minima, due to a lack of low frequencies in the data. A reflector below the zone of interest may, however, help in recovering the long-wavelength components of a velocity perturbation, as demonstrated in a paper by Mora. With the Born approximation for the perturbation in a reference model consisting of two homogeneous isotropic acoustic halfspaces, analytic expressions can be found that describe the spatial spectrum of the recorded seismic signal as a function of the spatial spectrum of the inhomogeneity. We study this spectrum in more detail by separately considering direct, reflected and head waves. Taking the reflection coefficient of the deeper reflector into account, we obtain sensitivity estimates for each of these types of waves. Although the head waves have a relatively small contribution to the reconstruction of the velocity perturbation, compared to the other waves, they contain reliable long-wavelength information that can be beneficial for full waveform inversion.

Introduction

Full waveform inversion (FWI) is increasingly more applied in seismic data processing. One important advantage of the method is that there is no need for data picking. A well-known drawback of FWI is the occurrence of local minima in the misfit functional. Bunks et al. (1995) showed that the availability of low frequencies in the recorded data improves the smoothness of the misfit functional and then reduces the number of local minima. In practice, however, these frequencies are absent from the data.

Diving-wave tomography (Woodward and Rocca, 1988; Pratt et al., 1996) can recover the large-scale structure of the velocity model if the initial velocity model is sufficiently close to the true model. Mora (1989) considered a velocity perturbation in a two-halfspace velocity model with a known constant velocity in the upper part below the surface where sources and receivers were located. He demonstrated that, in principle, FWI should be able to recover the long-wavelength structure of the velocity model by exploiting the transmission properties of the reflected waves. In his analysis, the reflector depths need not be known, since it is reconstructed by migration in the first FWI iteration. The improved illumination of the velocity perturbation by the reflected waves provides long-wavelength information that is lacking from the waves that were scattered back to the surface by the velocity perturbation.

Here, we extend his analysis by separately analyzing the refracted or head waves (Cerveny and Ravindra, 1971, e.g). If a reflector is smoothed, the distinction between refracted and diving waves disappears. The main question is if refracted waves will contribute to the long-wavelength part of the reconstructed velocity perturbation.

Background model

Figure 1 shows the problem that we will analyze. The 2-D background model consists of two isotropic, homogeneous acoustic halfspaces. Sources and receivers are assumed to be placed at every point on the line $z = 0$. All head waves have the same direction of propagation, as indicated in Figure 1. This means that there are only two incident directions from which the inhomogeneity is observed by the head waves (one direction is shown at the figure, the other is obtained by symmetry with respect to any vertical axis).

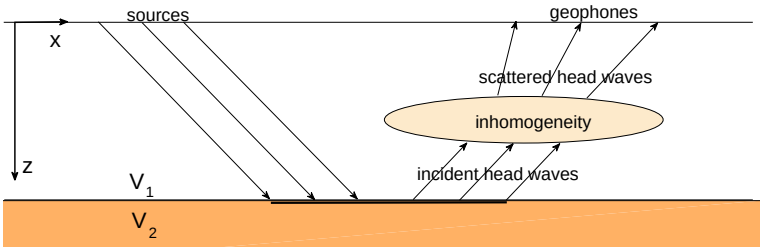

Figure 1 *Model problem and paths of the head waves*

Inversion method

The aim of our work is to investigate the effect of head waves on the inversion result. The Born approximation is used for the scattered field. After Fourier transforms in time and in the horizontal coordinates of sources and receivers, the wavefield perturbation is given by

$$\delta u_{sg}(k_s,k_g) = \int k^2 \tilde{f}_\omega(k_s)\delta W(\mathbf{r})G_s(k_s,\mathbf{r})G_g(k_g\mathbf{r})d\mathbf{r}. \qquad (1)$$

Here, $\tilde{f}_\omega$ is the source signature, $\delta W(\mathbf{r})$ is a relatively small perturbation of the background squared slowness, G_s is the source and G_g the receiver Green function for the background medium. The full wavefield perturbation as a function of the inhomogeneity becomes (Wu and Toksöz, 1987; Mora, 1989)

$$\delta u_{sg}(k_s,k_g) = -\frac{k^2\tilde{f}_\omega(k_s)}{4\gamma_{s1}\gamma_{g1}}[D_{(++)}\int \delta W(\mathbf{r})e^{i(\mathbf{s}_+ + \mathbf{g}_+)\cdot\mathbf{r}}d\mathbf{r} + D_{(+-)}C(k_g)\int \delta W(\mathbf{r})e^{i(\mathbf{s}_+ + \mathbf{g}_-)\cdot\mathbf{r}}d\mathbf{r}$$

$$+D_{(-+)}C(k_s)\int \delta W(\mathbf{r})e^{i(\mathbf{s}_-+\mathbf{g}_+)\cdot\mathbf{r}}d\mathbf{r}+D_{(--)}C(k_s)C(k_g)\int \delta W(\mathbf{r})e^{i(\mathbf{s}_-+\mathbf{g}_-)\cdot\mathbf{r}}d\mathbf{r}]. \qquad (2)$$

Using the analytical expression for the Green function of the background medium, the linear dependence between the full wavefield perturbation spatial spectrum and the inhomogeneity spatial spectrum is obtained:

$$\begin{aligned}\delta u_{sg}(k_s,k_g) \;\sim\; & \delta\widetilde{W}(\mathbf{s}_+ + \mathbf{g}_+) + C(k_g)\delta\widetilde{W}(\mathbf{s}_+ + \mathbf{g}_-) \\ & + C(k_s)\delta\widetilde{W}(\mathbf{s}_- + \mathbf{g}_+) + C(k_s)C(k_g)\delta\widetilde{W}(\mathbf{s}_- + \mathbf{g}_-). \end{aligned} \qquad (3)$$

Here $\delta\widetilde{W}(\mathbf{v}) = \int \delta W(\mathbf{r})e^{i(\mathbf{v}\cdot\mathbf{r})}d\mathbf{r}$ is a typical 2-D Fourier transformation of the squared slowness perturbation. $C(k_s)$ and $C(k_g)$ are the reflection coefficients for the respective monochromatic plane waves from the boundary between the halfspaces. The $D_{(..)}$ coefficients represent phase shifts along the wavepaths from the surface, where the sources and geophones are located, to the expected depth of the inhomogeneity. They are skipped in formula (3). The vectors are defined as

$$\mathbf{s}_\pm = \begin{pmatrix} k_s \\ \pm\gamma_{s1} \end{pmatrix}, \qquad \mathbf{g}_\pm = \begin{pmatrix} k_g \\ \pm\gamma_{s1} \end{pmatrix},$$

and the roots are $\gamma_{s1} = \sqrt{\omega^2/v_1^2 - k_s^2}$ and $\gamma_{s2} = \sqrt{\omega^2/v_2^2 - k_s^2}$. Figure 2 shows typical directions of source and geophone wavepaths passing through the centre of the inhomogeneity.

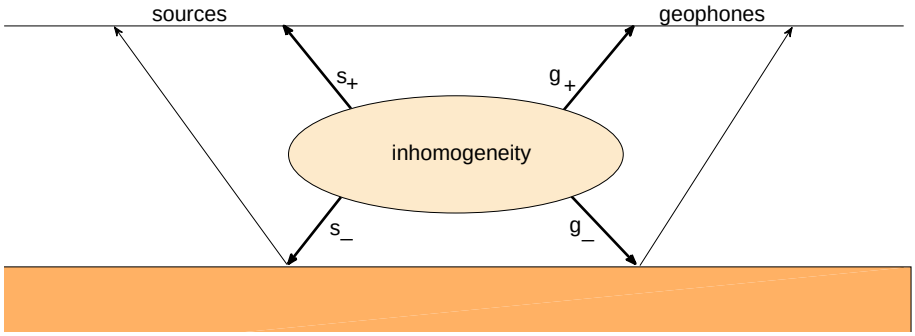

Figure 2 *Source and geophone wavepaths through the centre of the scatterer, described by the vectors* $\mathbf{s}_\pm$ *and* $\mathbf{g}_\pm$.

Equation (2) depends on the spatial Fourier transform of the squared slowness perturbation. Each term corresponds to different wave types. Those with branch points in the complex plane correspond to the head waves.

Results

The relation between the wavefield perturbation spatial spectrum and the inhomogeneity spatial spectrum is presented in the form of sensitivity diagrams, calculated for the full wavefield perturbation by

$$S_{full} = \left| \frac{\delta u_{sg}(k_s(k_x,k_z),k_g(k_x,k_z))}{\delta\widetilde{W}(k_x,k_z)} \right|, \qquad (4)$$

and for the head wavefield perturbation by

$$S_{head} = S_{full}\frac{|\delta u_{sg}^{head}(k_x,k_z)|}{|\delta u_{sg}^{head}(k_x,k_z)| + |\delta u_{sg}^{refl}(k_x,k_z)|} \simeq \left| \frac{\delta u_{sg}^{head}(k_s(k_x,k_z),k_g(k_x,k_z))}{\delta\widetilde{W}(k_x,k_z)} \right|. \qquad (5)$$

According to equation (2), we are able to construct points in the inhomogeneity spectrum $(\mathbf{s}_\pm + \mathbf{g}_\pm)$ which have an influence on the spectral amplitude for each point in the wave-field spectrum (k_s, k_g).

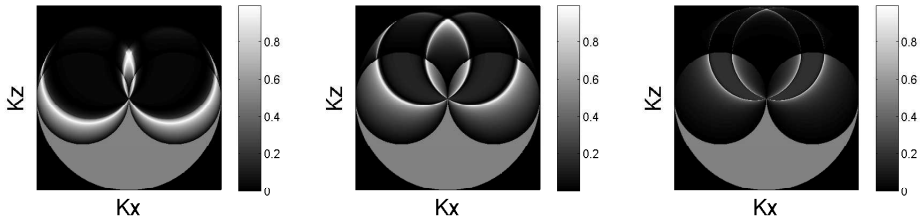

Figure 3 *Sensitivity diagrams for the head waves at different velocity contrasts, namely* $V_2/V_1 = 1.2$, 2, *and* 4, *from left to right, of the background velocity model.*

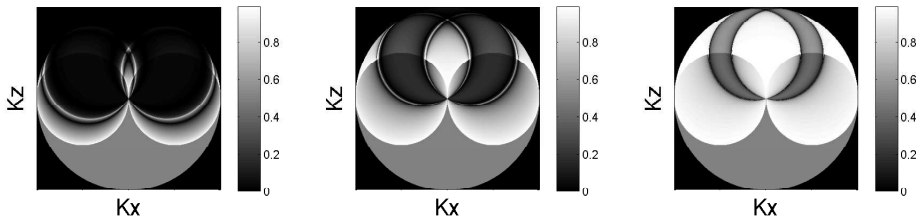

Figure 4 *As Fig. 3, but for the reflected waves.*

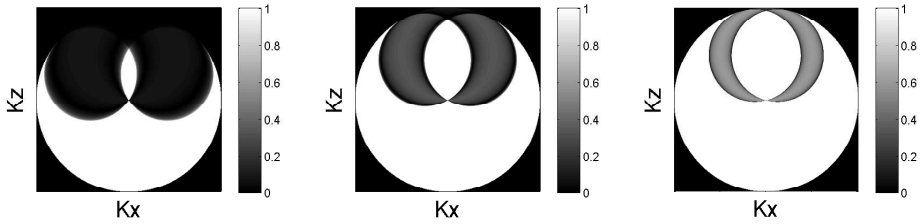

Figure 5 *As Fig. 3, but for the full wavefield*

However, for the diagrams of the sensitivity in terms of spectral coordinates of the inhomogeneity, it is much better to know the reverse transformation, meaning we should calculate (k_s, k_g) from (k_x, k_z). This transformation follows from

$$k_s + k_g = k_x, \quad \gamma_{s1} + \gamma_{g1} = k_z.$$

Figure 3 shows diagrams of the sensitivity of the head waves to the perturbations in the inhomogeneity spectrum for three velocity contrasts of the background model, using equation (5). For comparison, Figure 4 corresponds to the sensitivity of pure reflections.

$$S_{refl} = S_{full} \frac{|\delta u_{sg}^{refl}(Kx, Kz)|}{|\delta u_{sg}^{head}(Kx, Kz)| + |\delta u_{sg}^{refl}(Kx, Kz)|} \simeq \left| \frac{\delta u_{sg}^{head}(k_s(k_x, k_z), k_g(k_x, k_z))}{\delta \widetilde{W}(k_x, k_z)} \right|. \tag{6}$$

Figure 5 displays diagrams for the sensitivity of the full wavefield spectrum for the same parameters, using equation (4).

The values $\delta \widetilde{W}(k_x, k_z)$ from equation (4) are set to unity as they do not affect the sensitivity. Also, because the diagrams depend linearly on frequency through $k_x = \pm \frac{2\omega}{V_1}$ and $k_z = \pm \frac{2\omega}{V_1}$, we only have to consider a single frequency. Figures 6 and 7 compare the information content for reflections and head waves. They contain diagrams of the relative sensitivity defined by

$$S'_{head} = \frac{S_{head}}{S_{head} + S_{refl}}, \quad S'_{refl} = \frac{S_{refl}}{S_{head} + S_{refl}}. \tag{7}$$

The white regions correspond to maximum sensitivity, so the bright circles in Figure 6 mark part

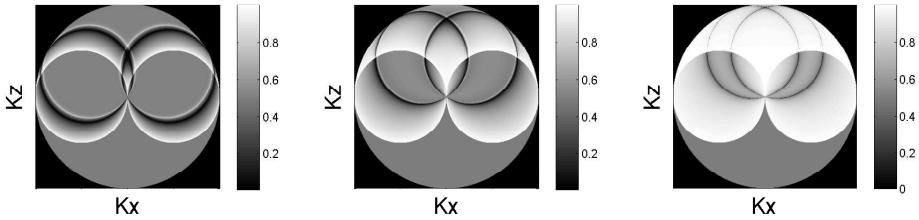

Figure 6 *Relative sensitivity diagrams for reflected waves.*

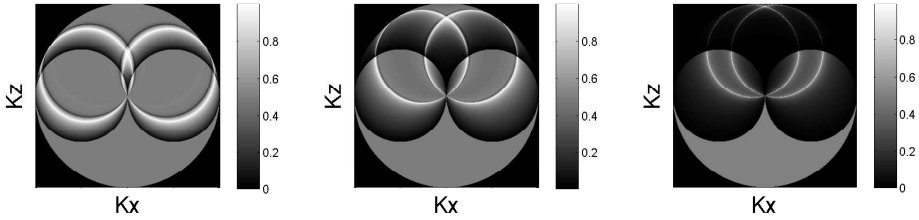

Figure 7 *Relative sensitivity diagrams for head waves.*

of the spectrum that can be recovered reliably by the head waves. As it turns out, these domains are rather small. However, although this part of the spectrum is small, it is important because it can not be reconstructed with pure reflections as the diagrams in Figure 7 show. Also, from the series of diagrams in Figures 6 and 7, we conclude that the lower the velocity contrast, the larger is the influence of head waves in comparison with pure reflections.

Conclusions

We have analyzed the contribution of head waves to the recovery of the spatial spectrum of a velocity inhomogeneity in FWI for a two-halfspace background model. It is impossible to recover the whole spectrum with head waves, but in a rather small part of spectrum they are more reliable than reflections. On the other hand, the frequencies in the spectrum of the head waves are lower than those for reflections and come closer to zero in the inhomogeneity spectrum. Also, the lower the velocity contrast of the deeper reflector, the larger is the relative contribution of head waves compared to pure reflections. Therefore, head waves can help FWI to reconstruct the long-wavelength structure of the velocity model.

Acknowledgements

The authors express their gratitude to Fons ten Kroode of Shell Global Solutions International BV for proposing and supporting this project.

References

Bunks, C., Saleck, F.M., Zaleski, S. and Chavent, G. [1995] Multiscale seismic waveform inversion. *Geophysics*, **60**(5), 1457–1473, doi:10.1190/1.1443880.

Cerveny, V. and Ravindra, R. [1971] *Theory of seismic head waves*. University of Toronto Press.

Mora, P. [1989] Inversion = migration + tomography. *Geophysics*, **54**(12), 1575–1586, doi:10.1190/1.1442625.

Pratt, R.G., Song, Z.M., Williamson, P.R. and Warner, M.R. [1996] Two-dimensional velocity models from wide-angle seismic data by waveform inversion. *Geophysical Journal International*, **124**(2), 323–340, doi: 10.1111/j.1365-246X.1996.tb07023.x.

Woodward, M.J. and Rocca, F. [1988] Wave-equation tomography. *SEG Technical Program Expanded Abstracts*, **7**(1), 1232–1235, doi:10.1190/1.1892498.

Wu, R.S. and Toksöz, M.N. [1987] Diffraction tomography and multisource holography applied to seismic imaging. *Geophysics*, **52**(1), 11–25, doi:10.1190/1.1442237.